IMMUNOLOGY

Endogenous DEL-1 restrains melanoma lung metastasis by limiting myeloid cell–associated lung inflammation

Young-Min Hyun[1]*, Sang-Uk Seo[2,3]*, Woo Seon Choi[4,5], Hyung-Joon Kwon[4], Dong-Young Kim[4], Soi Jeong[1], Gyeong-Yi Kang[1], Eunbi Yi[4,5], Minjung Kim[4], Hyun Jin Ryu[4], Mark R. Looney[6], Eun Young Choi[4†], Hun Sik Kim[4,5†]

Distant metastasis represents the primary cause of cancer-associated death. Pulmonary metastasis is most frequently seen in many cancers, largely driven by lung inflammation. Components from primary tumor or recruited leukocytes are known to facilitate metastasis formation. However, contribution of target site–specific host factor to metastasis is poorly understood. Here, we show that developmental endothelial locus–1 (DEL-1), an anti-inflammatory factor abundant in the lung and down-regulated by inflammatory insults, protects from melanoma lung metastasis independently of primary tumor development and systemic immunosurveillance. DEL-1 deficiency is associated with gene profiles that favor metastatic progression with inflammation and defective immunosurveillance. Mechanistically, DEL-1 deficiency primarily influences Ly6G$^+$ neutrophil accumulation in lung metastatic niche, leading to IL-17A up-regulation from γδ T cells and reduced antimetastatic NK cells. In support, neutrophil depletion or recombinant DEL-1 treatment profoundly reverses these effects. Thus, our results identify DEL-1 as a previously unrecognized link between tumor-induced inflammation and pulmonary metastasis.

INTRODUCTION

Metastatic tumors originating from malignant primary tumors are the leading cause of cancer-related mortality (~90%). Metastasis comprises a stepwise cascade encompassing the invasion and dissemination of the malignant cells followed by their colonization and adaptation to the microenvironment of the metastatic site. In these processes, an important determinant is tumor cell interactions with the host microenvironments, affecting host cell composition, cytokine milieu, and extracellular matrix (ECM) structures (*1*). In particular, distant metastasis to the target organ requires establishment of a favorable local microenvironment, termed the (pre)metastatic niche, for efficient colonization of the metastatic cells and their outgrowth (*1*, *2*). The contribution of various tumor-derived factors, consequent recruitment of bone marrow–derived cells (BMDCs), underlying ECM remodeling, and inflammation to metastatic niche formation is well documented (*2*–*4*). However, relatively little is known about target organ–specific host factors that contribute to shaping the metastatic microenvironment. This study would provide an important insight into metastatic niche formation and organ-specific metastatic tropism, which remains one of the key unresolved questions in cancer research (*2*, *5*).

Developmental endothelial locus–1 (DEL-1) is a secretory glycoprotein that is predominantly expressed by vascular endothelial cells in the lung and the brain and associates with the cell surface and the ECM (*6*, *7*). DEL-1 is also known as epidermal growth factor (EGF)–like repeats and discoidin I–like domains 3 (EDIL3) by virtue of its three N-terminal EGF-like repeats and two C-terminal discoidin I-like domains. DEL-1 interacts with phospholipids and distinct integrins, including αLβ2 (LFA-1; CD11a/CD18) and αMβ2 (Mac-1; CD11b/CD18) that are crucial to leukocyte adhesion, transmigration, and intraluminal crawling on the endothelium (*6*, *8*, *9*). Consistent with these characteristics, endothelial DEL-1 has recently emerged as a critical tissue homeostatic factor that regulates local inflammation by interfering with β2 integrin–dependent recruitment of leukocytes, predominantly neutrophils, to peripheral tissues (*6*). DEL-1–deficient mice exhibit an increased leukocyte infiltration and inflammatory pathologies in preclinical models of pulmonary inflammation and fibrosis (*7*, *10*). DEL-1 deficiency also aggravates disease severity of experimental autoimmune encephalomyelitis and inflammatory bone loss, accompanied by up-regulation of interleukin-17 (IL-17) and neutrophil infiltration (*11*, *12*). Given a causal link between inflammation and tumor progression, and being a regulator of local inflammation, it is feasible that tissue-derived DEL-1 modulates cancer metastasis. However, this possibility of metastasis control by local inflammatory regulator has not yet been addressed.

Among other organs with prominent DEL-1 expression, the lung is susceptible to inflammatory insults (*13*) and is a frequent metastatic site for different types of cancer, including melanoma, breast cancer, and lung cancer itself (*14*). Of particular interest is melanoma metastasis to the lung, given the preferential metastasis of lung-homing melanoma cells (*15*) and the strong association between inflammation and melanoma lung metastasis (*16*). DEL-1 has been recently implicated in primary tumor progression in a tumor cell–autonomous manner (*17*–*19*). These studies have centered on tumor-derived DEL-1 in certain cancer types and its potential contribution to proliferation, survival, and invasion of the cancer cells, using in vitro culture and an immunodeficient mouse model, without the assessment of tumor-host interactions. Thus, we sought to study the role of host DEL-1 in the formation of melanoma lung metastasis using syngeneic mouse models, focusing on immune cells in the metastatic niche that govern the balance between tumor escape versus elimination and thereby dictate metastatic outgrowth.

[1]Department of Anatomy and Brain Korea 21 PLUS Project for Medical Science, Yonsei University College of Medicine, Seoul, Republic of Korea. [2]Mucosal Immunology Laboratory, University of Ulsan College of Medicine, Seoul, Republic of Korea. [3]Department of Microbiology, College of Medicine, The Catholic University of Korea, Seoul, Republic of Korea. [4]Department of Biomedical Sciences, Asan Medical Center, University of Ulsan College of Medicine, Seoul, Republic of Korea. [5]Stem Cell Immunomodulation Research Center, Asan Medical Center, University of Ulsan College of Medicine, Seoul, Republic of Korea. [6]Departments of Medicine and Laboratory Medicine, University of California, San Francisco, San Francisco, CA, USA.
*These authors contributed equally to this work as first authors.
†Corresponding author. Email: choieun@ulsan.ac.kr (E.Y.C.); hunkim@amc.seoul.kr (H.S.K.)

RESULTS

DEL-1 deficiency aggravates lung metastasis but not primary melanoma growth

To study the effects of DEL-1 on melanoma lung metastasis, we used an experimental metastasis model of B16F10 melanoma cells. B16F10 cells injected via the tail vein primarily colonize the lung and develop metastatic foci within 2 weeks (*20*). B16F10 cells were labeled with DsRed to allow a sensitive and quantitative assessment of metastatic spread by means of fluorescence intensity (FLI) (fig. S1A). DEL-1–sufficient [wild-type (WT)] or –deficient (*Del1*KO) mice were then intravenously administered with the melanoma cells followed by the analysis of pulmonary metastatic growth. We found that *Del1*KO mice exhibited significantly more lung metastases than WT littermates, as measured by metastatic foci formation and fluorescence imaging (Fig. 1, A and B). Consistent with these findings, histologic examination of the lungs revealed increased nodule size and frequency of macrometastases (>1-mm diameter) in *Del1*KO mice (Fig. 1, C to E), suggesting more severe metastatic growth with DEL-1 deficiency. Similar results were also obtained at a lower tumor dose; *Del1*KO mice showed a significant increase in lung, but not liver, metastasis compared with WT mice (fig. S1, B to E), supporting the regulation of lung metastasis by DEL-1.

We next sought to determine whether DEL-1 also regulates the development of tumors at the orthotopic site. To this end, B16F10 cells expressing DsRed were implanted in the skin of the mice. There was no significant difference in the growth and weight of primary tumors over 3 weeks in *Del1*KO mice compared with WT mice (Fig. 1, F and G). However, a significant increase in spontaneous metastasis to the lung 3 weeks after inoculation, a time point of detectable melanoma seeding (*4*), was observed in *Del1*KO mice compared with WT mice (Fig. 1, H and I). This observation indicated that DEL-1 restrains melanoma lung metastasis but not primary tumor growth.

It has become clear that metastatic dissemination of tumor cells depends on escape from host immune surveillance (*21*). B16F10 melanoma cells are deficient in major histocompatibility complex (MHC) class I surface expression, as confirmed here (fig. S2A), and are preferentially targeted by natural killer (NK) cells that exert robust control on metastatic dissemination (*22*). Consistent with previous studies (*23*, *24*), systemic metastasis of B16F10 cells was mainly under the control of NK cells, as demonstrated by a substantial increase in

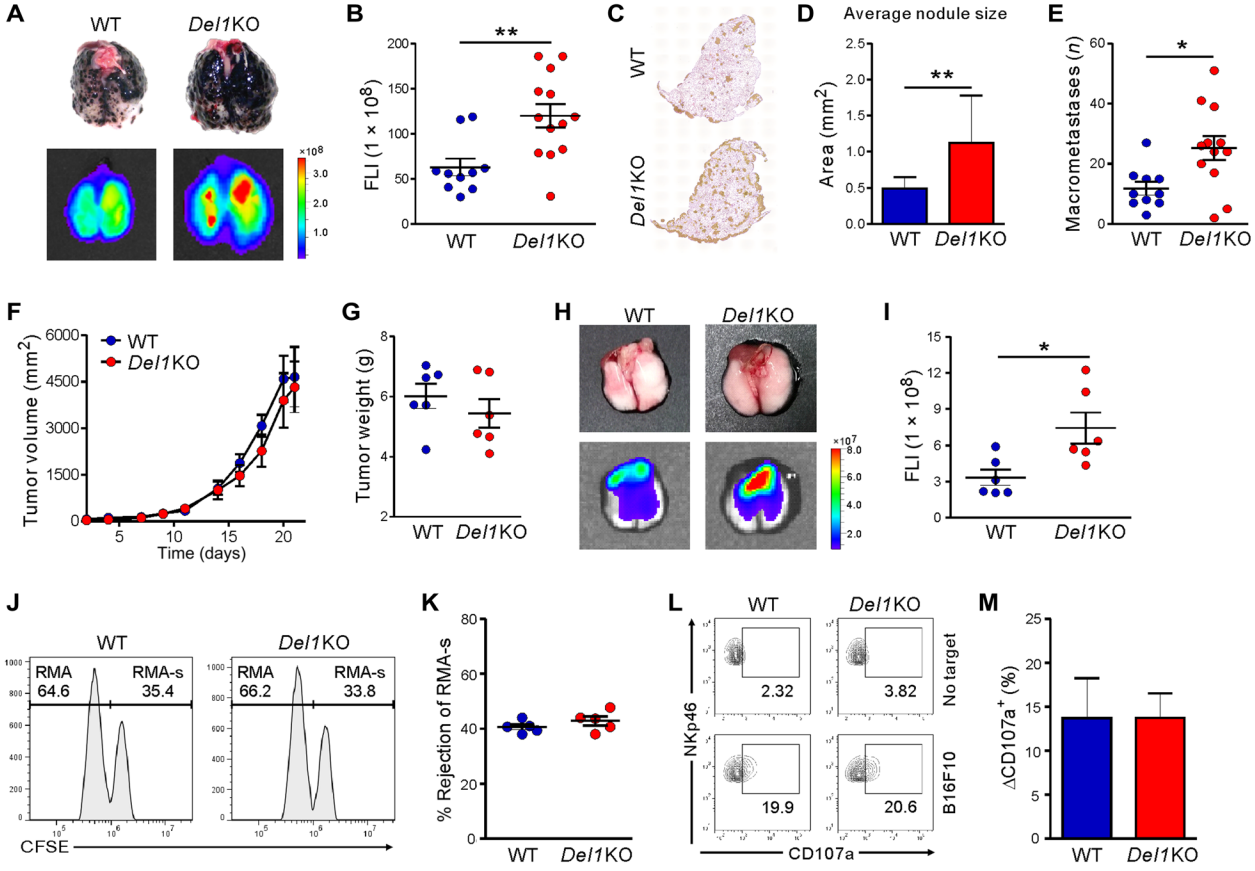

Fig. 1. Melanoma metastasis to the lung but not primary tumor growth is DEL-1 dependent. (**A** to **E**) WT ($n = 10$) or *Del1*KO ($n = 13$) mice were injected intravenously with 5×10^5 DsRed-B16F10 cells and analyzed for lung metastasis after 2 weeks. (A) Representative lung images (top) and corresponding DsRed fluorescence images (bottom). (B) Quantification of lung metastases by FLI depicted in (A). (C) Representative hematoxylin and eosin–stained lungs and (D) quantification of metastatic nodule size and (F) macrometastases from mice in (A). (**F** to **I**) DsRed-B16F10 cells were injected subcutaneously into WT and *Del1*KO mice ($n = 6$ per group). (F) Tumor sizes and (G) tumor weights were determined at the indicated time points and on day 21, respectively. (H) Representative lung images (top) and corresponding fluorescence images (bottom) showing spontaneous lung metastases. (I) Quantification of lung metastases by FLI depicted in (H). (**J** and **K**) Natural killer (NK) cell–mediated lymphoma clearance assay ($n = 5$ per group) showing representative result (J) and graph (K). (**L** and **M**) NK cell degranulation assay ($n = 6$ per group) showing representative result (L) and graph (M). $^*P < 0.05$; $^{**}P < 0.01$. Photo credits for (A) and (H): Hyung-Joon Kwon, University of Ulsan.

lung metastasis formation following NK cell depletion with anti–asialo-GM1 antibody but not CD4 or CD8 T cell depletion (fig. S2, B to E). NK cell depletion was also associated with an increase in liver metastasis (fig. S2, F and G), distinct from the effect of DEL-1 deficiency (fig. S1, D and E).

Thus, we studied whether DEL-1 deficiency is associated with an intrinsic defect in NK cell effector function. To assess systemic cytolytic activity of NK cells in vivo, we used a syngeneic lymphoma clearance model in which NK cells selectively kill MHC class I–deficient RMA-s cells over their parent MHC class I–intact RMA cells (*25*). We labeled RMA-s and RMA cells with high and low concentrations of carboxyfluorescein succinimidyl ester (CFSE) dye, respectively, and then coinjected equal numbers of the cells intraperitoneally into mice. Selective clearance of RMA-s cells over RMA cells was evident and comparable between WT and *Del1*KO mice (Fig. 1, J and K). Supporting the in vivo results, DEL-1 deficiency did not affect the cytolytic capacity of splenic NK cells against B16F10 (Fig. 1, L and M) or YAC-1 target cells (fig. S3, A and B). Moreover, DEL-1 deficiency had no effect on the cytotoxic activity of CD8 T cells upon stimulation with anti-CD3 antibody (fig. S3, C and D).

Given the prominent expression of DEL-1 in the endothelial barrier of the lung, these results suggest that DEL-1 deficiency has a localized effect on the control of lung metastasis that is independent of systemic immune surveillance.

DEL-1 deficiency affects gene expression profiles linked to inflammation and tumor immunity

To gain insight into pathogenetic mechanisms underlying the role of DEL-1 in metastasis, we next assessed the gene expression profile of the lung tissue of metastatic tumor-bearing mice. We focused on the tumor immune microenvironment using a polymerase chain reaction (PCR) array of 84 key genes associated with cancer inflammation and immunity cross-talk. Differentially expressed genes were identified as those up- or down-regulated by >2-fold in *Del1*KO mice compared with WT mice. Our analyses revealed that DEL-1 deficiency caused significant changes in several mediators and effectors of cross-talk between tumors and the immune system in the metastasis-bearing lung. DEL-1 deficiency was associated with an increased expression of genes related to tumor progression and metastasis (*Aicda*, *Hif1a*, *Bcl2l1*, and *Myc*), which correlated with down-regulation of genes involved in antitumor immunity (fig. S4). In line with these findings, similar decreases in expression were observed for genes encoding granzyme B (*Gzmb*; 1.9-fold), interferon-γ (*Ifng*; 1.91-fold), and its downstream targets (*Stat1*; 1.9-fold and *Gbp2b*). Of particular note was the increased expression in the gene encoding the p19 subunit of IL-23 (*Il23a*; 2.27-fold), which is linked to tumor-promoting chronic inflammation and suppression of tumor immune surveillance (*24*). Furthermore, there was an increase in gene expression (*Ccr1*, *Cxcr1*, and *Cxcr2*) related to the accumulation of tumor-associated myeloid cells that help establish an immunosuppressive microenvironment (*26*, *27*). Together with an intact immune surveillance by DEL-1–deficient NK cells, these results raise the possibility that DEL-1 deficiency may contribute to lung metastatic niche formation involving dysregulation of local immune homeostasis and inflammation.

DEL-1 deficiency leads to dysregulation of lung immune and inflammatory cell landscape

Having observed altered expression of genes encoding chemokine receptors, we evaluated whether DEL-1 deficiency could affect immune cell infiltration. Flow cytometry was used to analyze different leukocyte populations in the metastatic lung of WT and *Del1*KO mice (fig. S5). We found that the proportion of neutrophils, defined as $CD45^+CD11b^+Ly6G^+Ly6C^{int}$ and known to support metastatic progression (*28*, *29*), was significantly elevated in the metastasis-bearing lungs of *Del1*KO mice (Fig. 2, A and B) but not in the lungs of control tumor-free mice (fig. S6, A and B). These findings are compatible with the role of DEL-1 in the recruitment of neutrophils in inflammation-associated pathologies (*6*). By contrast, DEL-1 deficiency did not affect the infiltration of $CD11b^+Ly6G^-Ly6C^+$ monocytes, $CD11c^+F4/80^-MHCII^+$ dendritic cells, or $CD11b^+F4/80^+MHCII^+$ M1-like and $CD11b^+F4/80^+CD206^+$ M2-like macrophages among the $CD45^+$ cell populations. $CD3^-NK1.1^+$ NK cells that prevent B16F10 lung metastasis, but not other lymphocytes including $CD4^+$ T cells, $CD8^+$ T cells, and γδ T cells, were significantly decreased by DEL-1 deficiency (Fig. 2, A and B). These findings were supported by immunofluorescence analysis, which revealed a marked increase in the infiltration of $Ly6G^+$ neutrophils in the metastatic lungs of *Del1*KO mice, particularly at the peritumoral region, along with decreased infiltration of $NK1.1^+$ NK cells (Fig. 2C). Murine NK cells acquire effector function through a three-stage maturation program, which can be defined by differential surface expression of CD11b and CD27 ($CD11b^-CD27^+$, $CD11b^+CD27^+$, and fully mature $CD11b^+CD27^-$) (*30*). We observed a comparable frequency of all these subsets in metastasis-bearing lungs of WT and *Del1*KO mice, suggesting that functional NK cell maturation was not affected by DEL-1 deficiency (Fig. 2, D and E). Furthermore, there was no significant difference in the frequency of leukocyte populations, particularly neutrophils, in the spleen, liver, and peripheral blood, all absent in DEL-1 expression (*7*), between WT and *Del1*KO mice bearing B16F10 lung metastases (fig. S6, C to H). These findings provide further evidence for a preferential effect of DEL-1 on the recruitment of leukocytes to the lung of tumor-bearing mice.

DEL-1 deficiency promotes melanoma metastasis to the lung in a neutrophil-dependent manner

Next, we assessed whether the increased neutrophils were functionally important in melanoma lung metastasis of *Del1*KO mice. Neutrophils were depleted using anti-Ly6G antibody before and after intravenous injection of B16F10 cells expressing DsRed. We found that lung metastasis was significantly decreased by $Ly6G^+$ neutrophil depletion, as assessed by metastatic foci formation and fluorescence imaging (Fig. 3, A and B). Efficacy of neutrophil depletion was confirmed in the lungs of treated mice (Fig. 3, C and D). This depletion led to a significant accumulation of NK cells, along with $Ly6C^+$ monocytes. In addition, we observed an increase in mature cytotoxic NK cells ($CD11b^+CD27^-$) but a decrease in immature NK cells ($CD11b^-CD27^+$) (Fig. 3, E and F). Thus, these results suggest a negative regulation of NK cell homeostasis by neutrophils in the metastasis-bearing lung, an observation compatible with the prometastatic role of neutrophils via suppression of NK cell–mediated tumor cell clearance (*31*).

We then investigated the possible mechanisms underlying the increased neutrophil accumulation associated with lung metastasis in *Del1*KO mice. DEL-1 deficiency has been linked to enhanced lymphocyte production of IL-17 (*11*, *12*), a cytokine that promotes neutrophil mobilization and expansion (*27*). IL-23, where we found the mRNA up-regulation of its subunit in the metastasis-bearing lungs of *Del1*KO mice (fig. S4), enhances IL-17 production in $CD4^+$ T cells and γδ T cells (*32*). In support, IL-17A expression was significantly

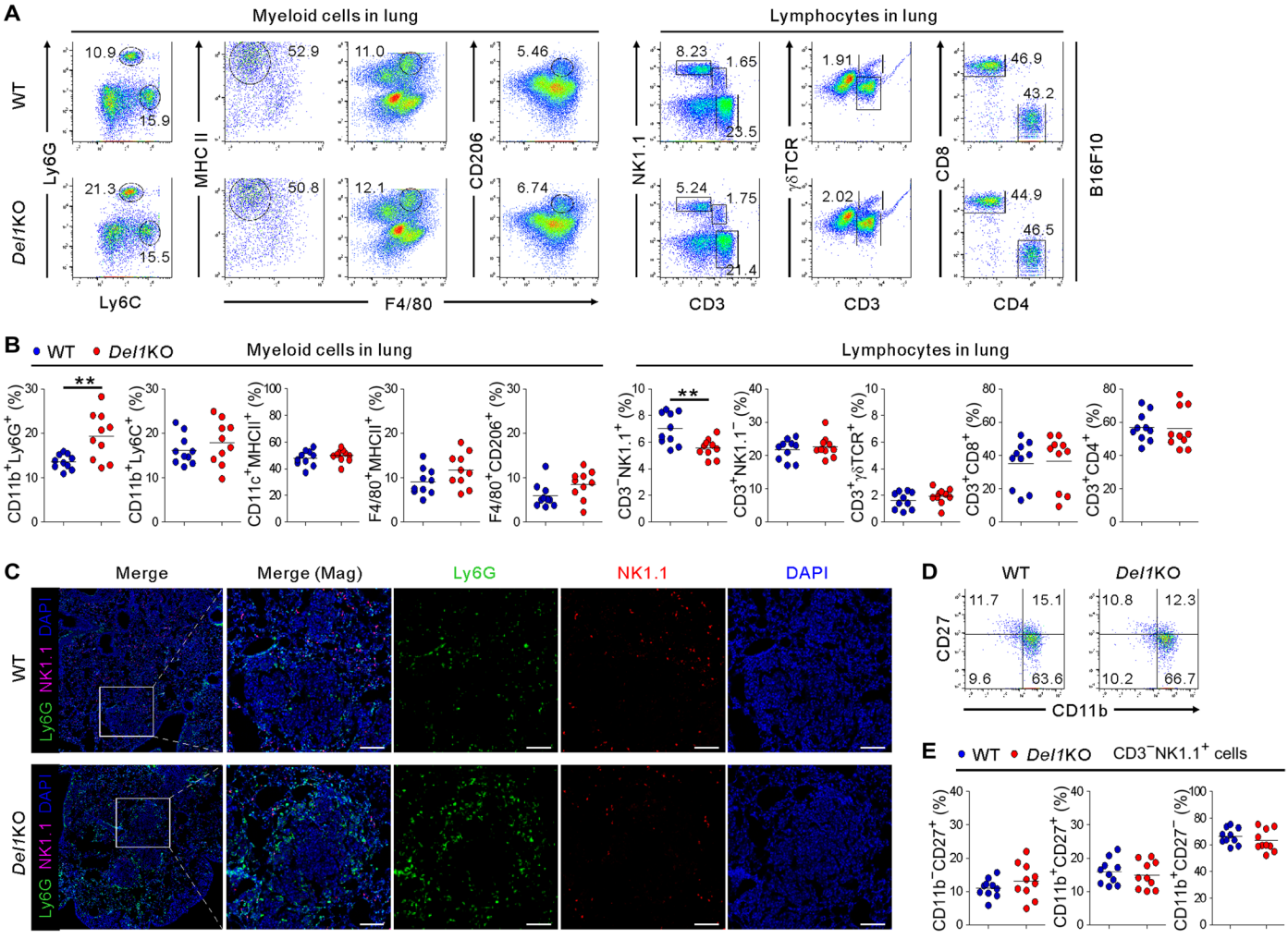

Fig. 2. Reciprocal regulation of Ly6G$^+$ neutrophils and NK cells by DEL-1 in the metastasis-bearing lung. (**A** and **B**) Representative (A) and quantitative (B) flow cytometric analysis of various myeloid cells (CD11b$^+$Ly6G$^+$ neutrophils, CD11b$^+$Ly6C$^+$, monocytes, CD11c$^+$MHCII$^+$ dendritic cells, and F4/80$^+$MHCII$^+$ M1-like and F4/80$^+$CD206$^+$ M2-like macrophages) and lymphocytes (CD3$^-$NK1.1$^+$ NK cells, CD3$^+$γδ T cells, CD8$^+$ T cells, and CD4$^+$ T cells) among CD45$^+$ cell populations in the metastasis-bearing lungs of WT and *Del1*KO mice ($n = 10$ each group) on day 14 after intravenous injection of B16F10 cells. (**C**) Representative immunofluorescence staining for Ly6G and NK1.1 in a metastasis-bearing lung from each group of mice depicted in (A). Ly6G$^+$ (green) neutrophils and NK1.1$^+$ (red) NK cells with 4′,6-diamidino-2-phenylindole (DAPI) counterstain (blue) are shown. Magnified images (right panel for each mouse group) show peritumoral localization of Ly6G$^+$ neutrophils. Scale bars, 100 μm. (**D** and **E**) Representative (D) and quantitative (E) flow cytometric analyses of CD11b and CD27 expression on NK1.1$^+$ NK cells in the metastasis-bearing lungs of WT and *Del1*KO mice ($n = 10$ each group) depicted in (A). Horizontal bars indicate the means (B and E). $^{**}P < 0.01$.

increased by γδ T cells but not CD4$^+$ or CD8$^+$ T cells in the metastasis-bearing lungs of *Del1*KO mice (Fig. 3, G and H), and the increase was diminished by Ly6G$^+$ neutrophil depletion (Fig. 3, I and J). These results support the clear link between IL-17–producing γδ T cells and neutrophils in the tumor context (*29*, *33*). To further probe the role of IL-17 in neutrophil accumulation and melanoma metastasis to the lung, mice were administered recombinant IL-17A during lung metastasis formation. IL-17A–treated mice exhibited a significant increase in the number of metastatic foci in the lungs, which was comparable to that of *Del1*KO mice (fig. S7A). Furthermore, immunohistochemical analysis revealed diminished DEL-1 expression in the lungs, particularly in the vasculature, along with Ly6G$^+$ neutrophil accumulation (fig. S7, B and C), which was consistent with IL-17–mediated repression of DEL-1 expression (*34*). Moreover, it appeared that the expression of DEL-1 along with CD31 became gradually lost at the peritumoral region during metastatic progression in WT mice (fig. S7D), consistent with neutrophil accumulation at the peritumoral region (Fig. 2C and fig. S7C). These results suggest a potential link among tumor-induced inflammation, DEL-1 deficiency, and neutrophil accumulation. This notion was further supported by the reduced mRNA expression of DEL-1 during metastasis formation in the WT mice (fig. S7E). Collectively, our results suggest a protective role for DEL-1 in limiting neutrophil accumulation and thereby melanoma metastasis to the lung via an effect on IL-17$^+$ γδ T cells.

Administration of Del-1-Fc ameliorates lung metastasis

To further probe the antimetastatic function of DEL-1, we assessed the effect of recombinant DEL-1 treatment on neutrophil accumulation and lung metastasis. Del-1-Fc fusion protein has been shown

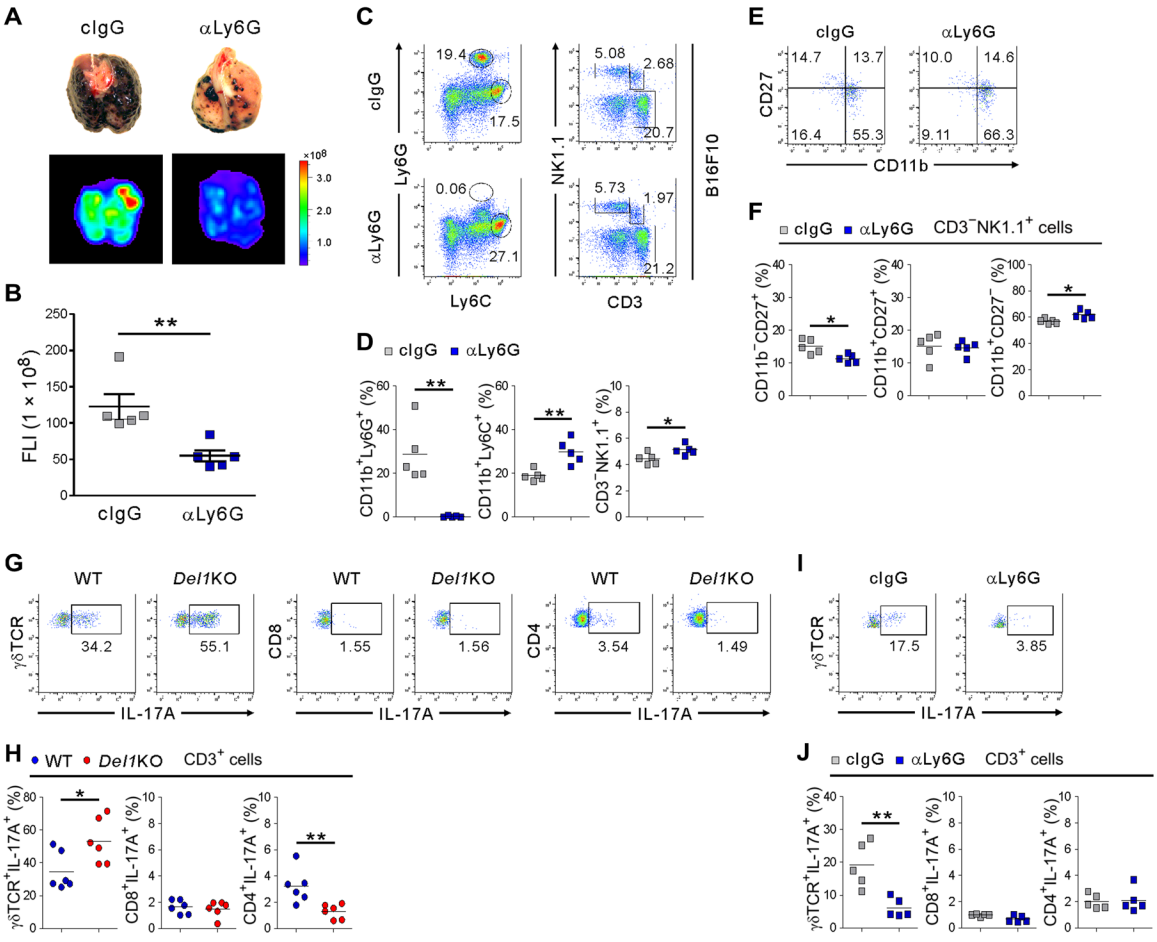

Fig. 3. DEL-1 deficiency promotes melanoma lung metastasis in a neutrophil-dependent manner. (**A**) Representative lung images (top) and corresponding DsRed fluorescence images (bottom) showing the diminished metastases to the lungs of *Del1*KO mice ($n = 5$ per group) treated with anti-Ly6G antibody. Photo credit: Hyung-Joon Kwon, University of Ulsan. (**B**) Quantification of lung metastases by FLI depicted in (A). (**C** and **D**) Representative (C) and quantitative (D) flow cytometric analysis of myeloid cells and lymphocytes, graphed on Ly6C by Ly6G and CD3 by NK1.1 dot plots, respectively, among $CD45^+$ cell populations in the metastasis-bearing lungs depicted in (A). (**E** and **F**) Representative (E) and quantitative (F) flow cytometric analysis of CD11b and CD27 expression on $NK1.1^+$ NK cells depicted in (A). (**G** and **H**) Representative (G) and quantitative (H) flow cytometric analysis of intracellular IL-17A expression in different lymphocytes in the metastasis-bearing lung of WT and *Del1*KO mice ($n = 6$ per group). (**I** and **J**) Representative (I) and quantitative (J) flow cytometric analysis of intracellular IL-17A expression in different lymphocytes depicted in (A). Horizontal bars indicate the means (D, F, H, and J). $^*P < 0.05$; $^{**}P < 0.01$.

to circulate and reduce neutrophil-mediated inflammatory pathologies (*11*, *12*). WT mice were treated intravenously on a regular basis with either Del-1-Fc or control-Fc during lung metastasis formation. Prophylactic administration of Del-1-Fc significantly attenuated melanoma lung metastasis (Fig. 4, A and B), accompanied by reduced neutrophil accumulation (Fig. 4, C and D). Del-1-Fc administration after tumor inoculation also alleviated melanoma lung metastasis (fig. S8, A and B) and neutrophil accumulation (fig. S8, C and D), suggesting the effect of DEL-1 during metastasis formation. These results support the notion that DEL-1 has a protective role against metastatic progression.

DEL-1 regulates lung metastatic niche formation

We next sought to elucidate the steps in the metastatic cascade affected by DEL-1 deficiency. Given that there was no difference in primary tumor growth between WT and *Del1*KO mice (Fig. 1, F and G), we focused on the post-intravasation steps of the metastatic cascade. To this end, we used an experimental metastasis model to circumvent the confounding effects of primary tumor-associated systemic as well as lung inflammation (*2*, *16*, *35*). To facilitate the identification of the inoculated B16F10 cells, they were labeled with XenoLight DiR fluorescent dye that enables in vivo imaging of cell homing. WT or *Del1*KO mice were then intravenously administered with the labeled B16F10 cells followed by the analysis of their trapping in various organs. DEL-1 deficiency did not affect the numbers of B16F10 cells that extravasate or seed in different organs including the lung, when evaluated by FLI up to 24 hours (fig. S9). Thus, DEL-1 deficiency might contribute to enhanced colonization of metastatic cells after initial seeding, which relies on lung metastatic niche.

Accordingly, we evaluated whether DEL-1 deficiency could affect the survival and proliferation of disseminated tumor cells in the lung during metastasis formation. To facilitate B16F10 cell identification, metastasis-bearing lungs were examined after intravenous

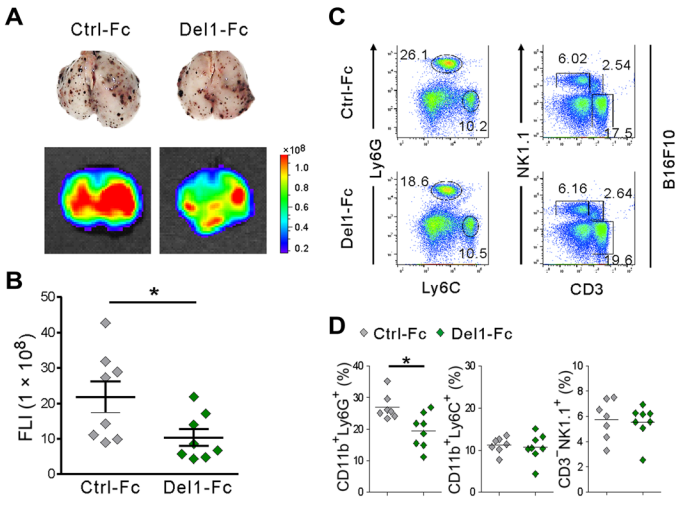

Fig. 4. Melanoma lung metastasis and neutrophil accumulation are ameliorated by Del-1-Fc administration. (**A** and **B**) C57BL/6 mice were treated with intravenous injection of control-Fc or Del-1-Fc 6 hours before an intravenous injection of 2×10^5 B16F10 cells expressing DsRed and twice a week treatment thereafter. (A) Representative lung images (top) and the corresponding DsRed fluorescence images (bottom) showing lung metastases ($n = 8$ each group) after 14 days of tumor implantation. Photo credit: Hyung-Joon Kwon, University of Ulsan. (B) Quantification of lung metastases by FLI depicted in (A). (**C** and **D**) Representative (C) and quantitative (D) flow cytometric analysis of different myeloid cells and lymphocytes, graphed on Ly6C by Ly6G and CD3 by NK1.1 dot plots, respectively, in the metastasis-bearing lungs depicted in (A). Horizontal bars indicate the means (D). *$P < 0.05$.

injection of DsRed-tagged B16F10 cells. DEL-1 deficiency did not affect the proportion of proliferating B16F10 cells relative to total B16F10 cells, as demonstrated by the immunohistochemical staining for Ki67, a widely used proliferation marker (fig. S10A). By comparison, the percentage of TUNEL-positive apoptotic B16F10 cells was significantly lower in metastasis-bearing lungs of *Del1*KO mice compared with WT mice (fig. S10B). This decrease in cell death was further confirmed by flow cytometric analysis of DsRed-tagged B16F10 cells after LIVE/DEAD dye staining (fig. S10C) and was associated with an attenuated cytotoxicity of NK cells in the metastasis-bearing lungs of *Del1*KO mice (fig. S10D). Treatment of B16F10 cells with Del-1-Fc had no direct effect on their proliferation and survival (fig. S10, E and F). Thus, these results suggest an impaired NK cell–mediated clearance of B16F10 cells as a potential mechanism of aggravated metastatic burden by DEL-1 deficiency, consistent with a decrease in NK cells in the metastasis-bearing lungs of *Del1*KO mice (Fig. 2, A and B).

Given a local defect in NK cells linked to neutrophil accumulation in DEL-1–deficient lung metastatic niche, we speculated that DEL-1 primarily affects neutrophils rather than NK cells. Thus, we investigated the effect of DEL-1 on leukocyte recruitment at early metastatic time points. Metastatic tumors are able to induce BMDC recruitment to the sites targeted for metastasis to form a metastatic niche, supportive of tumor cell colonization (*4*, *35*). This phenomenon can be mimicked by the administration of tumor-conditioned medium (CM) alone without tumor cell inoculation (*4*). Thus, tumor-free mice were intravenously injected with cell-free CM derived from B16F10 melanoma cells (Fig. 5A). Compared with WT mice, *Del1*KO mice showed a significant increase in the frequency of neutrophils, but not of monocytes or lymphocytes examined, in the CM-treated lungs (Fig. 5, B and C). This increased recruitment of neutrophils was not observed in the spleen (Fig. 5, D and E). Next, we asked whether CM pretreatment modulates metastatic outcome upon tumor inoculation. Thus, we repeated the above experiment of CM treatment, followed by intravenous injection of luciferase-labeled B16F10 melanoma cells. We observed a significant increase in lung metastasis, as measured by bioluminescence imaging (BLI), in CM-treated WT mice (Fig. 5, F and G), compatible with an increase of neutrophils in CM-treated lungs (Fig. 5, B and C) relative to control lungs (fig. S6, A and B) of WT mice and a previous study (*4*). In comparison, the same treatment had a less significant effect in *Del1*KO mice, suggesting that the prometastatic effect of CM was likely compensated by DEL-1 deficiency–associated neutrophil accumulation in lung metastatic niche (Fig. 2, A and B). DEL-1–dependent local accumulation of neutrophils was also observed in the lung, but not blood and BM, of mice following systemic treatment with granulocyte-macrophage colony-stimulating factor (GM-CSF) and IL-6 (fig. S11, A and B). These cytokines are involved in the expansion, mobilization, or recruitment of myeloid cells including prometastatic neutrophils to the tumor site (e.g., lung) (*36*–*39*). In addition, DEL-1 deficiency did not affect the in vitro expansion of myeloid cells upon treatment of BM cells with GM-CSF and IL-6 (fig. S11, C and D). Thus, our results collectively suggested that DEL-1 primarily regulates the accumulation of $Ly6G^+$ prometastatic neutrophils in the lung metastatic niche that facilitates the metastatic progression.

DEL-1 limits the recruitment of neutrophils to lung metastatic foci

To better understand DEL-1–dependent neutrophil trafficking in lung metastasis, we examined the spatiotemporal dynamics of neutrophil recruitment to early metastatic foci via two-photon intravital imaging. LysM–green fluorescent protein (GFP) mice were used to enable visualization of neutrophils that express GFP brightly compared with monocytes and thus are readily identified as clear GFP^+ cells (*40*, *41*). Moreover, it is known that more neutrophils than monocytes extravasate (*42*). The imaging experiments were performed after formation of metastatic foci via intravenous injection of DsRed-B16F10 cells (Fig. 6A). Compared with WT mice, *Del1*KO mice showed a significant increase in the number of neutrophils extravasated into the lungs, particularly around metastatic foci (Fig. 6, B and C, and movie S1). Analysis of the neutrophil migration trajectory toward melanoma foci revealed that more neutrophils swarmed to the metastatic foci from the longer distance by DEL-1 deficiency (Fig. 6D and movies S2 and S3). Supporting this, DEL-1 deficiency was related to significantly higher velocity (Fig. 6E) and longer distance, termed displacement (Fig. 6F), of neutrophil migration toward metastatic foci. However, DEL-1 deficiency did not affect the movement trajectory, termed meandering index (Fig. 6G). The increased migration of neutrophils was associated with significantly enhanced adhesion of neutrophils to the luminal side of blood vessels (fig. S12). This result is compatible with a previous study showing the increased firm adhesion of leukocytes to the blood vessels in *Del1*KO mice using intravital imaging of the dorsal skin (*7*). We next investigated whether the increased migration of neutrophils was attributed to DEL-1 deficiency in neutrophils. Specifically, WT and *Del1*KO neutrophils were labeled with CMTPX [4(or 5)-(4-(chloromethyl)benzamido)-2-(1,2,2,4,8,10,10,11-octamethyl-1,2,10,11-tetrahydropyrano[3,2-g:5,6-g']diquinolin-13-ium-6-yl)benzoate] (red) and CMFDA (5-chloromethylfluorescein diacetate) (green),

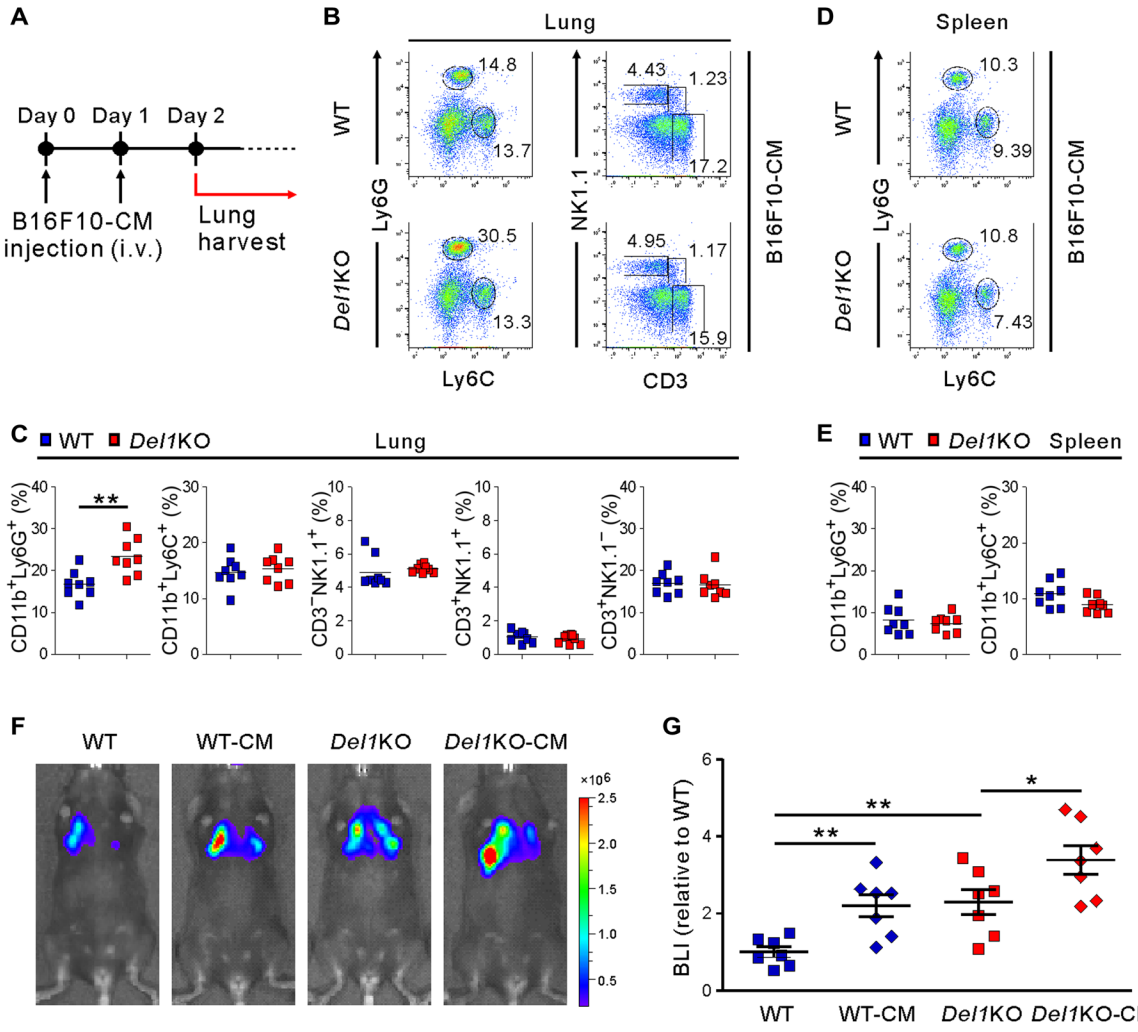

Fig. 5. CM from B16F10 cells induces neutrophil accumulation in the lung microenvironment. (**A**) Schematic diagram showing the schedule for B16F10-CM treatment. WT and *Del1*KO mice ($n = 8$ each group) were intravenously administered with B16F10-CM for two consecutive days. Mice were euthanized the next day after the last B16F10-CM treatment. (**B** and **C**) Representative (B) and quantitative (C) flow cytometric analysis of myeloid cells and lymphocytes, graphed on Ly6C by Ly6G and CD3 by NK1.1 dot plots, respectively, among $CD45^+$ cell populations in the lungs depicted in (A). (**D** and **E**) Representative (D) and quantitative (E) flow cytometric analysis of myeloid cells, graphed on Ly6C by Ly6G dot plots, among $CD45^+$ cell populations in the spleens depicted in (A). (**F** and **G**) Representative images (F) and quantification (G) of lung metastasis in WT or *Del1*KO mice ($n = 7$ each group) after administration of media or B16F10-CM as depicted in (A) and then injection of B16F10-Luc2 cells by luciferase-based bioluminescence imaging (BLI). One day after the last B16F10-CM treatment, mice received an intravenous injection of B16F10-Luc2 cells. Horizontal bars indicate the means (C and E). $^*P < 0.05$; $^{**}P < 0.01$.

respectively, or vice versa for their identification, and then equal numbers of cells were coinjected intravenously into the metastasis-bearing lungs of *Del1*KO mice. The analysis using two-photon intravital imaging revealed that the migration of WT neutrophils was comparable to that of *Del1*KO neutrophils (fig. S13, A and B, and movie S4). In support, DEL-1 deficiency in neutrophils did not affect their adhesion to and transmigration through *Del1*KO endothelial cells (fig. S13, C and D). Thus, these data suggest the role of DEL-1 in endothelial cells, but not neutrophils, in the regulation of neutrophil trafficking into the metastasis-bearing lung.

Furthermore, we performed three-dimensional (3D) imaging of metastasis-bearing lung after optical tissue clearing to enable the anatomical location of neutrophils and metastatic cells in tissues and blood vessels to be distinguished throughout the 3D structure of the lung. Analysis of 3D imaging revealed the metastatic foci to be mainly localized in the tissue and not in the blood vessels (Fig. 6H and movie S5). Furthermore, the number of extravasated neutrophils close to metastatic foci (<50 μm), but not that of tumor-infiltrating neutrophils, was significantly increased by DEL-1 deficiency (Fig. 6, I and J, movie S6). Thus, our results collectively suggest that DEL-1 deficiency promotes the recruitment of neutrophils into the lung to surround metastatic foci, possibly creating a permissive microenvironment for metastatic growth of disseminated tumor cells.

DISCUSSION

The lung is a frequent site of metastatic colonization from diverse extrapulmonary malignancies, which is linked to its susceptibility to inflammatory insults (*13*, *16*, *38*). However, the molecular mechanism of such metastatic vulnerability remains largely elusive. Herein,

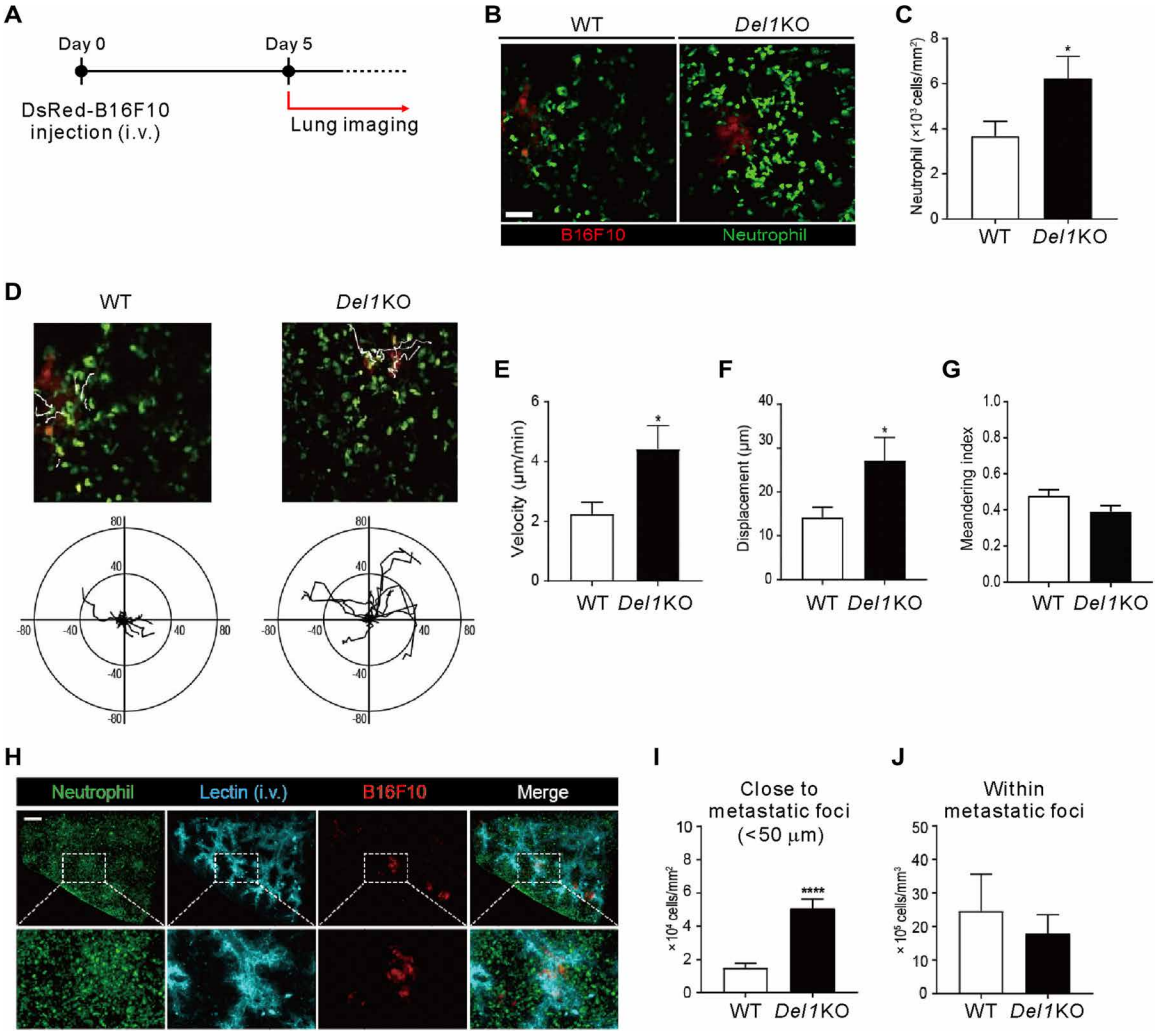

Fig. 6. DEL-1 deficiency promotes neutrophil recruitment to perimetastatic foci in the lung. (**A**) Scheme of two-photon intravital imaging. DsRed-B16F10 cells were intravenously injected (day 0) and imaged at day 5 for GFP^+ neutrophils and $DsRed^+$ B16F10 cells. (**B** and **C**) Representative images (B) and quantification (C) of neutrophils around metastatic foci in the lungs of LysM-GFP/WT ($n = 10$) or LysM-GFP/*Del1* KO mice ($n = 7$). Scale bar, 50 μm. (**D**) Migration trajectories of neutrophils observed for 15 min in a field of view. The starting point for each neutrophil was set to zero. Axis unit = μm. (**E** to **G**) Quantification of neutrophil velocity (E), displacement (F), and meandering index (G) from intravital imaging. (**H**) Broad view of cleared lung tissue 5 days after DsRed-B16F10 cell injection. Scale bar, 300 μm. (**I**) Counts of neutrophils within 50 μm from the boundaries of metastatic foci. (**J**) The number of neutrophils inside the metastatic foci. $^*P < 0.05$; $^{****}P < 0.0001$.

we first demonstrated DEL-1, an exemplar of a local inflammatory regulator with prominent expression in the lung, as a critical regulator of melanoma lung metastasis. DEL-1 restrains metastatic spread of malignant melanoma to the lung, but not primary tumor growth, through a significant effect on leukocyte recruitment, particularly by attenuating $Ly6G^+$ neutrophils, and IL-17A expression by γδ T cells. We showed that depletion of $Ly6G^+$ cells in such a context reverses the prometastatic effect of DEL-1 deficiency and IL-17A dysregulation. A local, but not systemic, control of metastasis by DEL-1 was further supported by finding altered inflammatory infiltrates centered on neutrophils in the lung metastatic niche, but comparable metastatic seeding of melanoma and intrinsic function of systemic NK cells. Together with reciprocal regulation between DEL-1 and IL-17A and their correlation with neutrophil recruitment, these findings suggest that DEL-1 acts as a local gatekeeper protecting from lung inflammation and associated metastasis formation.

Neutrophils are among the "first responders" to be recruited to the lung to mediate an inflammatory response against infection or tissue damage and have also emerged as key contributors to the formation of the lung metastatic niche (*13*, *27*, *28*). Metastatic colonization and progression are provoked by neutrophil-associated systemic as well as local lung inflammation (*16*, *38*). Although circulating neutrophils may exert antimetastatic cytotoxicity depending on the context (*43*), neutrophils in the tumor microenvironment are reported to undergo phenotypic changes and acquire the ability to promote metastasis, in part, by dampening the antitumor immunity provided by cytotoxic cells (*29*, *31*, *44*). In this study, DEL-1 deficiency was associated with an elevation of prometastatic neutrophils in the metastasis-bearing lung, along with a decrease in antimetastatic NK cells. This is reminiscent of the dependence of neutrophil recruitment on DEL-1 in different inflammatory pathologies but, as demonstrated here, in a tumor metastatic setting. Moreover, the

finding of reduced metastasis in conjunction with restored NK cells via depletion of Ly6G$^+$ cells suggests that DEL-1 primarily affects prometastatic neutrophil accumulation in the lung metastatic niche. This notion was supported by the preferential accumulation of neutrophils among BMDCs in the DEL-1–deficient lungs following CM challenge and treatment with GM-CSF and IL-6. While we demonstrated the dispensable role of DEL-1 in neutrophils and NK cells in our metastasis model, DEL-1 may also affect other leukocytes linked to metastatic outcome. In this regard, it merits further investigation using DEL-1 conditional knockout mouse targeting specific cell types to confirm our results.

DEL-1 deficiency is causally linked to IL-17–mediated inflammatory pathologies, and infiltrating leukocytes are the main producers of IL-17 (*11*, *12*). Supporting this, DEL-1 deficiency led to an elevation of IL-17A–producing γδ T cells in metastasis-bearing lungs. Expansion and polarization of prometastatic or protumorigenic neutrophils are driven by IL-17$^+$ γδ T cells (*29*, *33*), which represent an important source of IL-17 in mucosal tissues including the lung (*12*, *33*). Consistent with this, local IL-17A administration herein could recapitulate in WT mice the increased accumulation of neutrophils and melanoma lung metastasis by DEL-1 deficiency. We found that Ly6G$^+$ cell depletion led to a significant reduction in tumor-induced IL-17$^+$ γδ T cells, implying that prometastatic neutrophils support the generation of IL-17A–producing γδ T cells. Given previous studies showing that IL-17$^+$ γδ T cells promote neutrophil accumulation, we speculate that there exists a positive-feedback loop between IL-17$^+$ γδ T cells and neutrophils in the process of metastatic progression, which could be interrupted by the local anti-inflammatory factor DEL-1. In this regard, further studies would be required to address the exact mechanisms underlying the relationship among DEL-1 deficiency, neutrophil accumulation, IL-17$^+$ γδ T cells, and lung metastasis.

Distinct from the role of host endothelial DEL-1 in metastasis suppression as shown here, previous studies have centered on the tumor-intrinsic role of DEL-1 in primary tumor progression (*17*–*19*). As such, DEL-1, albeit to variable extent of expression in certain cancer cell lines and tumor tissues, was linked to tumor cell proliferation, survival, and invasion. On the basis of these findings, targeting of tumor-derived DEL-1 has been considered a potential therapeutic strategy to suppress tumor progression. However, using immunocompetent syngeneic mouse models herein, we found that melanoma lung metastasis was facilitated by DEL-1 deficiency, pointing to an opposite function of host DEL-1 over tumor-intrinsic DEL-1. This speculation was further supported by an antimetastatic effect of Del-1-Fc administration. Thus, given the crucial role of the immune system in tumor progression and metastasis, caution would be required to consider DEL-1 as a target for cancer therapy, particularly in cases of primary or metastatic tissues with prominent endogenous DEL-1 expression.

In summary, here, we demonstrate the previously unappreciated antimetastatic effect of DEL-1 on melanoma lung metastasis via limiting neutrophil accumulation beyond its defined role as a local inflammatory regulator in diverse inflammatory disorders. In this regard, it is tempting to speculate that DEL-1 could restrain the development of pulmonary metastasis from other cancers. In support, we observed a similar aggravation of lung metastasis by DEL-1 deficiency in a neutrophil-dependent manner using an experimental metastasis model of TC-1 lung cancer cells (fig. S14). To validate and extend our findings to other cancer types, further studies in a different lung metastasis model, including another model of metastatic melanoma, will be required. One issue of great interest that remains to be addressed is the clinical relevance of the results in this study. In primary melanoma, neutrophil infiltration is associated with poor prognosis (*45*), whereas metastatic primary melanomas with a high NK score are linked to better patient survival (*46*). Given the neutrophil accumulation along with NK cell decrease as a feature of DEL-1–deficient metastatic lungs, it is our belief that DEL-1 may affect the melanoma lung metastasis and patient prognosis. Thus, the relationship between lung-resident DEL-1 and melanoma metastatic outcome warrants further investigation. In addition to the lung, brain and bone, where functional expression of DEL-1 is demonstrated, are also major organs targeted by metastasis. Thus, studying the role of DEL-1 in the regulation of metastatic progression therein merits further investigation. In addition, investigation of other local inflammatory regulators that are potentially tailored to specific tissues in the context of tumor development and metastasis formation will also be of interest.

MATERIALS AND METHODS

Study design

The objective of this study was to investigate the role of local tissue-derived factor, DEL-1 herein, in the regulation of pulmonary metastasis, given the focus of previous studies on the components derived from primary tumor or recruited leukocytes to the metastatic niche. The contribution of DEL-1 to melanoma lung metastasis was analyzed by both experimental and spontaneous models of metastasis using syngeneic immunocompetent mice and B16F10 melanoma cells expressing DsRed that enable a quantitative assessment of metastatic spread. This approach was distinct from previous studies that are confined to the role of tumor cell–derived DEL-1 in promoting their own proliferation and invasion, using an immunodeficient mouse model, without the assessment of tumor-host interactions. Lung and other tissues and host cells were obtained for the analyses of gene expression, fluorescent imaging, flow cytometry, (immuno) histological staining, and intravital and 3D imaging. A series of in vivo and in vitro experiments allowed us to identify a significant role of DEL-1 in protection from melanoma lung metastasis via limiting the recruitment of prometastatic neutrophils in lung metastatic niche, which was strengthened by the intravital and 3D imaging of neutrophils. A reasonable sample size was chosen to ensure adequate reproducibility of the results and to achieve statistical significance, which was based on our previous studies related to DEL-1. No animal data were excluded. Mice were assigned according to their genotype. Age/sex-matched littermates were used whenever possible. In in vivo experiments, investigators were blinded to the genotype of the experimental groups. Mouse samples were labeled as numeric numbers and analyzed in a blinded manner. Biological and technical replicates have been performed. Most of the experiments have been reproduced two to three independent times with comparable results. The experimental findings, particularly DEL-1–mediated suppression of melanoma lung metastasis, have been reproduced with similar results from three independent laboratories and are shown with representative data.

Mice

*Del1*KO mice on a C57BL/6 background (*7*) were provided by T. Chavakis (Dresden University, Germany). Six- to eight-week-old

littermates were used for tumor model experiments. C57BL/6 mice were purchased from Orient Bio (Seongnam, Korea). Animals were fed ad libitum and kept under specific pathogen–free conditions. All experimental protocols were approved by the Institutional Animal Care and Use Committee of the Asan Institute for Life Sciences. *Del1* KO mice were crossed with mice heterozygous for GFP expressed under the lysozyme-M promoter (LysM-GFP) (*40*) to generate LysM-GFP/WT or LysM-GFP/*Del1* KO mice. Six- to eight-week-old littermates were used for intravital imaging and tissue clearing. Mice were maintained in the Avison Biomedical Research Center (ABMRC) of Yonsei University College of Medicine. All experimental protocols were approved by the Institutional Animal Care and Use Committee of the Yonsei University College of Medicine (IACUC No. 2019-0097).

Cell culture and reagents

B16F10 and B16F10-Luc2 melanoma cell lines [American Type Culture Collection (ATCC)] were cultured in Dulbecco's modified Eagle's medium (DMEM) supplemented with 10% fetal bovine serum (FBS) and harvested for tumor model experiments using Detachin Cell Detachment Solution (Gelantis). TC-1 lung cancer cell line was cultured in RPMI 1640 medium supplemented with 10% FBS and 2 mM L-glutamine. YAC-1 (ATCC), RMA, and RMA-s murine lymphoma cell lines were cultured in RPMI 1640 medium supplemented with 5% FBS and 2 mM L-glutamine. P815 (ATCC) cell line was cultured in IMDM (Iscove's Modified Dulbecco's Medium) medium supplemented with 10% FBS and 2 mM L-glutamine. Plat-A retroviral packaging cell line (Cell Biolabs) was cultured in DMEM supplemented with 10% FBS, puromycin (1 μg/ml), and blasticidin (10 μg/ml). DsRed-tagged B16F10 cells were generated by transducing B16F10 cells with DsRed retroviral construct (Addgene). Retroviral particles were produced by transfection of Plat-A retroviral packaging cell line with pMXs-DsRed Express. B16F10 cells were transduced with virus-containing supernatant by spinfection in the presence of polybrene (4 μg/ml). Thereafter, B16F10 transductants showing DsRed expression were selected by fluorescence-activated cell sorting (FACS) and grown as pure cultures. DsRed-tagged TC-1 cells were generated by the same strategy as described for DsRed-B16F10 cells. Human Del-1-Fc fusion protein (Del-1-Fc) purified from human embryonic kidney 293 F cells (EDIL3-C-Fc) and control-Fc were purchased from Y-Biologics (Daejeon, Korea). Recombinant human IL-2 was obtained from Roche; recombinant murine IL-17A was purchased from PeproTech; recombinant murine GM-CSF and IL-6 were obtained from R&D Systems; CFSE, CellTrace Far Red Cell Proliferation Kit, and LIVE/DEAD Fixable Green Dead Cell Stain were acquired from Molecular Probes; and XenoLight DiR NIR fluorescent dye was obtained from PerkinElmer.

Mouse tumor model

To generate models of primary tumor growth and spontaneous metastasis, 1×10^6 DsRed-tagged B16F10 cells in 100 μl of Dulbecco's phosphate-buffered saline (DPBS) were subcutaneously injected into the shaved flank of mice. Tumor volume was measured using digital calipers and calculated as $V = (L \times W^2)/2$. After 3 weeks of primary tumor growth, lung metastases were measured by ex vivo fluorescence imaging of excised lungs using the In Vivo Imaging System (IVIS) Lumina II (PerkinElmer) platform. For experimental metastasis, DsRed-tagged B16F10 cells or unlabeled B16F10 cells (2×10^5 or 5×10^5 cells) in 200 μl of medium containing 5% FBS were injected into mice via the tail vein. Pulmonary metastases were assessed by histologic, gene expression profile, flow cytometric, and fluorescence imaging analyses on day 7 or 14 after tumor cell injection. For experiments monitoring extravasation and seeding, B16F10 cells were incubated with XenoLight DiR dye (320 μg/ml in DPBS) for 30 min at 30°C. Then, 5×10^5 cells were injected into mice via the tail vein, and initial seeding in lungs, livers, and spleens collected 30 min to 24 hours afterward was assessed by detecting XenoLight DiR–positive tumor cells using an IVIS Lumina II system.

Depletion of NK cells, T cells, and neutrophils

To deplete NK cells, mice received intraperitoneal injections of 10 μl of rabbit anti–asialo-GM1 (Cedarlane Laboratories Ltd.) while the control mice were injected with rabbit serum (Sigma-Aldrich). The injections were performed 1 day before an intravenous injection of B16F10 cells and then twice a week until euthanasia. To deplete $CD4^+$ or $CD8^+$ T cells, mice were intraperitoneally injected with anti-CD4 (150 μg per mouse, clone GK1.5; Bio X Cell) or anti-CD8 antibody (150 μg per mouse, clone 2.43; Bio X Cell) 1 day before an intravenous injection of B16F10 cells, and then twice a week thereafter. Matching isotype rat IgG2b (clone LTF-2; Bio X Cell) was used as a control. To deplete neutrophils, mice were intraperitoneally injected with anti-Ly6G antibody (150 μg per mouse, clone 1A8; Bio X Cell) 1 day before an intravenous inoculation of B16F10 cells, and then thrice a week thereafter. Matching isotype rat immunoglobulin G2a (IgG2a) (clone 2A3; Bio X Cell) was used as a control. The depletion of NK cells, CD4 and CD8 T cells, and neutrophils was confirmed by flow cytometry.

NK cell–mediated lymphoma clearance assay

To assess whether DEL-1 deficiency affects systemic NK cell activity in vivo, a lymphoma clearance assay was performed as previously described (*24*). Briefly, lymphoma cells expressing MHC class I (RMA) or defective MHC class I (RMA-s) were labeled with 1 and 4 μM CFSE, respectively. The cells were mixed in a 1:1 ratio (1×10^6 cells per each cell type) and injected intraperitoneally into WT or *Del1*KO mice. After the 6-hour challenge of RMA:RMA-s cells, the rejection of NK cell–sensitive RMA-s relative to NK cell–resistant RMA cells in the peritoneal cavity was measured using flow cytometry and calculated as follows: $1 - ([CFSE^{low}/CFSE^{high}]\text{input}/[CFSE^{low}/CFSE^{high}]\text{output}) \times 100\%$.

NK cell and $CD8^+$ T cell degranulation assay

Cytotoxic degranulation was assessed by measuring cell surface expression of CD107a as previously described (*47*). Resting or IL-2–activated NK cells isolated from splenocytes by negative selection using a mouse NK cell isolation kit (STEMCELL Technologies) were stimulated with YAC-1 or B16F10 cells for 4 hours. Lymphocytes were gated on forward scatter/side scatter, and the CD107a expression of $CD3\varepsilon^-NKp46^+$ NK cells was analyzed by flow cytometry. NK cell degranulation was determined by the percent increase of $CD107a^+$ NK cells after stimulation with YAC-1 or B16F10 cells relative to $CD107a^+$ NK cells without stimulation ($\Delta CD107a^+$ cells). For assessing $CD8^+$ T cell-cytotoxic activity, IL-2–activated $CD8^+$ T cells were isolated from splenocytes by negative selection using a mouse $CD8^+$ T cell isolation kit (STEMCELL Technologies) and were stimulated with P815 cells preincubated with anti-CD3ε antibody (10 μg/ml, clone 145-2C11; BioLegend) or isotype control antibody (10 μg/ml,

clone HTK888; BioLegend) for 4 hours. P815 cells are FcR^+ and serve as a classical target for T cell cytotoxicity via their ability to bind antibodies to specific activating receptors (for example, CD3ε). In doing so, they can stimulate T cells through CD3ε. Cytotoxic degranulation was measured by surface expression of CD107a on $CD3\varepsilon^+CD8a^+$ T cells after lymphocyte gate.

Flow cytometry and intracellular staining

Lungs were perfused and removed from euthanized mice. Then, single-cell suspensions were obtained by incubating chopped tissues with collagenase II (1 mg/ml) (Sigma-Aldrich), collagenase IV (Worthington), and deoxyribonuclease I (50 U/ml) (Roche) for 30 min at 37°C using a gentleMACS Octo Dissociator (Miltenyi Biotec). Isolated cells were washed, treated with red blood cells lysis buffer (eBioscience), and filtered through a 70-μm strainer. Cell suspensions were preblocked with mouse BD Fc Block (clone 2.4G2), incubated with LIVE/DEAD Fixable Aqua Dead Cell Stain (Molecular Probes), and then incubated with conjugated antibodies. For intracellular staining of IL-17A, cell suspensions were stimulated with phorbol 12-myristate 13-acetate (20 ng/ml; Sigma-Aldrich), ionomycin (1 μg/ml; Sigma-Aldrich), and GolgiPlug (BD Biosciences) for 3 hours at 37°C, followed by staining for surface markers. Cells were then fixed, permeabilized, and stained for IL-17A. The following antibodies were used for staining: anti–CD45-eFluor 780 (clone 30-F11), anti–CD11b-PE (phycoerythrin)–Cy7 (clone M1/70), anti–Ly6G-PerCP-Cy5.5 (clone 1A8), anti–Ly6C-APC (allophycocyanin) (clone AL-21), anti–F4/80-FITC (fluorescein isothiocyanate) (clone BM8), anti–CD11c-PE (clone HL3), anti–MHC II-PerCP-Cy5.5 (clone M5/114.15.2), anti–CD206-APC (clone C068C2), anti–CD3ε-PerCP (clone 145-2C11), anti–NK1.1-PE (clone PK136), anti–CD27-FITC (clone LG.7F9), anti–CD4-APC (clone RM4-5), anti–CD8a-PE (clone 53-6.7), anti–γδTCR-FITC (clone GL3), anti–IL-17A-PE-Cy7 (clone eBio17B7), anti–NKp46-PE (clone 29A1.4), anti–CD107a-FITC (clone 1D4B), and anti–MHC I-PE (clone AF6-88.5). Labeled cell populations were measured using a BD FACSCanto II (BD Biosciences), and data were analyzed using FlowJo version 10 (Tree Star). To analyze the survival of DsRed-tagged B16F10 cells during lung metastasis formation, single-cell suspensions (2×10^5 cells) in the metastasis-bearing lungs of WT and *Del1*KO mice were stained with LIVE/DEAD Fixable Green Dead Cell Stain at room temperature (RT) for 30 min. B16F10 cells were gated on forward scatter/side scatter, and the LIVE/DEAD-stained dead cells of total DsRed-positive B16F10 cells were analyzed by flow cytometry.

NK cell cytotoxicity assay

To assess NK cell cytotoxicity in the metastasis-bearing lungs of WT and *Del1*KO mice, CellTrace Far Red-labeled B16F10 cells (1×10^4 cells) were cocultured with lung single cells (1×10^5 cells) for 6 hours at 37°C in the 96-well V bottom plate (Nunc). For the spontaneous death control, CellTrace Far Red-labeled B16F10 cells were cultured alone under the same conditions. Thereafter, cells were stained with the LIVE/DEAD Fixable Green Dead Cell Stain at RT for 30 min. B16F10 cells were gated on forward scatter/side scatter, and the LIVE/DEAD stain–positive dead cells among Far Red–labeled B16F10 cells were analyzed by flow cytometry.

In vitro myelopoiesis assay

Bone marrow cells were harvested from femurs and tibia of WT and *Del1*KO mice under sterile conditions. Cells were filtered through a 70-μm strainer and cultured in 24-well plates (5×10^5 cells per well) for 4 days in RPMI 1640 medium supplemented with 10% FBS, 10 mM Hepes, and 50 μM 2-mercaptoethanol. Recombinant GM-CSF (10 ng/ml) and IL-6 (10 ng/ml) were added in the cultures. Treatment media were changed every other day. On day 4, the frequency of different myeloid cells was analyzed by flow cytometry.

In vivo GM-CSF and IL-6 administration

To assess the effects of GM-CSF and IL-6 on the mobilization of myeloid cells, WT and *Del1*KO mice were intraperitoneally injected with recombinant GM-CSF (20 μg/kg) and IL-6 (20 μg/kg) daily for three consecutive days. After 4 days, mice were euthanized, and the cells from bone marrow, blood, or lung tissue were harvested for flow cytometry analysis of different myeloid cells.

RT^2 Profiler PCR Arrays

Metastatic lung tissues were excised and placed immediately into RNAlater solution (Invitrogen) for RNA extraction. Thereafter, total RNA was isolated from the lung tissue using an RNeasy Microarray Tissue Mini Kit (Qiagen). As previously described (*48*), quantitative reverse transcription (RT)–PCR was used to measure the relative amounts of 84 different mRNAs in the lung tissue by using mouse Cancer Inflammation and Immunity Crosstalk RT^2 Profiler PCR Arrays (Qiagen/SA Biosciences). cDNA was synthesized from 2 μg of total RNA using SuperScript III reverse transcriptase (Invitrogen). Then, RT-PCR was performed using SuperArray Master Mix (Qiagen) and a Roche LightCycler 480 instrument, according to the manufacturer's instructions. Experiments were performed on RNA pooled from three to four individual mice per group.

Quantitative RT-PCR

Real-time RT-PCR was performed in metastatic lung tissues isolated from WT mice or mice injected with B16F10 cells. Total RNA was isolated using QIAzol (Qiagen), and cDNA was synthesized using the High-Capacity cDNA RT Kit (Applied Biosystems/Thermo Fisher Scientific). The cDNA was amplified using LightCycler 480 SYBR Green 1 master in a LightCycler 480 machine (Roche). The following PCR conditions were used: 95°C for 15 min; 45 cycles of 30 s at 95°C, 30 s at 60°C, and 30 s at 72°C; and 95°C for 15 min. Melting curve analysis was conducted for all PCR products to ensure primer specificity. DEL-1 mRNA levels were normalized to 18*S* mRNA levels, and relative transcript levels were determined using the comparative C_T method. Sequences of the primer used are as follows: DEL-1 forward primer: 5′-CTT GGT AGC AGC CTG GCT TT-3′; DEL-1 reverse primer: 5′-GCC TTC TGG ACA CTC ACA GG-3′; 18*S* forward primer: 5′-CGC GGT TCT ATT TTG TTG GT-3′; and 18*S* reverse primer: 5′-AGT CGG CAT CGT TTA TGG TC-3′.

Histologic analysis and immunohistochemistry

To analyze metastatic foci formation in the lungs, the mice were euthanized, and the lung was fixed in Fekete's solution. The metastatic foci were assessed using a dissecting microscope (Nikon). The lung was also fixed with 4% paraformaldehyde, dehydrated, and then embedded in paraffin. Serial paraffin-embedded sections (4 μm) were stained with hematoxylin and eosin (H&E). Slides after H&E staining were scanned with the Vectra slide scanner (PerkinElmer) to quantify the metastatic area, and the spectral library of hematoxylin was created. Then, inForm image analysis software (PerkinElmer) was applied to quantify the spectra in the lung tissues. To detect

$Ly6G^+$ neutrophils in the metastatic lungs, frozen sections (12 μm) were incubated with primary antibody against Ly6G (1:100, 1A8; BD Biosciences) for 1 hour and stained using a Vectastain ABC kit (peroxidase, rat IgG; Vector Laboratories). The diaminobenzidine (DAB) signal was observed using the DAB substrate kit (Roche) and then imaged with a DM IL microscope (Leica).

Immunofluorescence

To detect neutrophils and NK cells in the metastatic lungs, serial frozen sections (12 μm) were prepared and incubated with primary antibodies against Ly6G (1:100, 1A8; BD Biosciences) and NK1.1 (1:100, PK136; BD Biosciences) for 1 hour followed by Alexa Fluor 488–conjugated goat anti-rat F(ab′)2 (1:250; Jackson ImmunoResearch) and Alexa Fluor 647–conjugated goat anti-mouse F(ab′)2 (1:250; Jackson ImmunoResearch) for 30 min in PBS containing 1% bovine serum albumin and 1% goat serum. All incubations were performed under coverslips at RT, followed by three washes with PBS. Nuclei were stained with 4′,6-diamidino-2-phenylindole (DAPI) (Molecular Probes), and coverslips were mounted with ProLong Gold Antifade Reagent (Molecular Probes). Cells were imaged with an LSM 710 laser-scanning confocal microscope (Carl Zeiss). To analyze DEL-1 expression by endothelial cells in the metastatic lungs, frozen sections (15 μm) were prepared, permeabilized with 0.1% Triton X-100 in PBS, and incubated with rabbit anti-mouse DEL-1 (1:200; AbFrontier) and Alexa Fluor 594–conjugated anti-mouse CD31 (1:200, MEC13,3; BioLegend) for 12 hours at 4°C, followed by Alexa Fluor 488–conjugated goat anti-rabbit IgG (1:500; Invitrogen) for 1 hour. Coverslips were mounted with Fluoromount-G (Electron Microscopy Sciences) after DAPI staining and then imaged with an LSM 710 confocal microscope. Regions of interest were randomly selected from the areas surrounding tumor foci. Protein expression was semiquantified from all images taken with the same settings after adjustments (exposure time, signal amplification, and objectives), using ImageJ software (NIH). To detect proliferation of B16F10 cells expressing DsRed in the metastasis-bearing lungs, serial frozen sections (15 μm) were prepared and incubated with primary antibody specific for Ki67 (1:500, ab15580; Abcam), followed by Alexa Fluor 488–conjugated goat anti-rabbit IgG (1:500; Invitrogen). Nuclei were stained with DAPI (Invitrogen). Proliferating B16F10 cells were identified as $DsRed^+Ki67^+$ cells. To detect apoptotic B16F10 cells expressing DsRed in the metastasis-bearing lungs, the frozen sections were subjected to terminal deoxynucleotidyl transferase–mediated deoxyuridine triphosphate nick end labeling (TUNEL) assay using a DeadEnd Fluorometric TUNEL System kit (Promega) according to the manufacturer's protocol. TUNEL-positive B16F10 cells were imaged with an LSM 710 laser-scanning confocal microscope.

In vitro proliferation and apoptosis assay

To assess the effect of DEL-1 on the proliferation of B16F10 cells, CFSE-labeled B16F10 cells were treated with control-Fc or Del-1-Fc (100 nM) for 48 hours and then subjected to flow cytometric analysis of cell division by dilution of CFSE. To assess the effect of DEL-1 on cell viability, B16F10 cells were treated with control-Fc or Del-1-Fc (100 nM) for 3 days, stained with propidium iodide and fluorochrome-conjugated annexin V, and then analyzed by flow cytometry.

Conditioned media assay

CM was prepared from B16F10 cells (5×10^6 cells) cultured in serum-free DMEM in 10-cm plates (Nunc) for 24 hours. Harvested CM was centrifuged and filtered (0.22-μm filter, Millipore) to remove cell debris. To study BMDC lung infiltration, CM (300 μl) was injected intravenously into WT or *Del1*KO mice for two consecutive days, and lungs were harvested the next day for flow cytometry analysis. To assess the effect of CM on melanoma lung metastasis, WT or *Del1*KO mice were treated with CM as described above and then subjected to tail vein injection of luciferase-tagged B16F10-Luc2 cells (5×10^5 cells) on the next day. Pulmonary metastases were assessed on day 14 after tumor cell injection using bioluminescent imaging (IVIS Lumina II system). Luminescence was normalized to day 0 for each individual mouse to account for any differences in injection efficiency of B16F10 cells between mice.

Neutrophil adhesion and transmigration assays

Adhesion of mouse neutrophils isolated from bone marrow onto isolated and cultured mouse vascular lung endothelial cells was performed as previously described (*7*). Briefly, purified and cultured lung endothelial cells from *Del1*KO mice were incubated in a microtiter plate (Nunc) until confluence. Fluorescence (BCECF)-labeled WT or *Del1*KO neutrophils (1×10^5 cells per well) were plated onto the endothelial cell monolayer and incubated at 37°C for 30 min. Following incubation periods and washing, the fluorescence of input and adherent cells was determined using a fluorescence plate reader (BioTek, Synergy HT). To assess transmigration of neutrophils through endothelial cells, primary endothelial cells were plated onto transwell culture inserts (SPL Life Sciences, 8-μm pore size) and incubated until confluence. WT or *Del1*KO neutrophils (1×10^5 cells per well) were added to the upper chamber. The lower chamber contained serum-free medium and recombinant IL-8 (5 ng/ml; R&D systems). After incubation for 50 min, the cells in the lower chamber were harvested and analyzed using LUNA-II Automated Cell Counter (Logos Biosystems Inc., Korea).

Two-photon intravital imaging

Two-photon intravital imaging was performed to observe neutrophil migration and melanoma tumor metastasis in the lung. For imaging, LSM 7MP microscope (Carl Zeiss Microscopy, Jena, Germany) equipped with a two-photon laser (690 to 1040 nm, MaiTai HD DeepSee tunable laser) was used. Morphology and motility of neutrophils were assessed at 880-nm wavelength in LysM-GFP/WT or LysM-GFP/*Del1*KO mice intravenously injected with DsRed-tagged B16F10 cells. Neutrophils (bright green) and monocytes (dim green) were readily distinguishable due to their distinct brightness levels and morphological features (*49*). To induce metastatic foci in the lung, 3×10^6 DsRed-B16F10 cells in 100 μl of PBS were intravenously injected 5 days before imaging. To compare the extravasation of WT and *Del1*KO neutrophils through *Del1*KO vascular endothelial cells, neutrophils were prepared from WT or *Del1*KO mice using mouse neutrophil enrichment kit (STEMCELL Technologies, Vancouver, Canada). Thereafter, WT and *Del1*KO neutrophils were labeled with CellTracker CMTPX (red) and CellTracker CMFDA (green) (Thermo Fisher Scientific, Waltham, MA, USA), respectively, or vice versa. The labeled neutrophils were mixed in a 1:1 ratio (3×10^6 cells per each genotype) and injected intravenously into *Del1*KO mice 5 days after inoculation of 3×10^6 B16F10 cells. Then, two-photon intravital imaging was performed to count the WT and *Del1*KO neutrophils recruited to the metastasis-bearing lung of *Del1* KO mice. For visualizing blood flow, Texas Red-dextran (70 kDa; Thermo Fisher Scientific, Waltham, MA, USA)

was intravenously injected. Lung imaging was performed via a thoracotomy of anesthetized mice, as previously described (*50*). Anesthesia was performed using Zoletil-Rompun mixture diluted 1:10 in PBS before surgery.

Tissue clearing

Mice intravenously injected with DsRed-B16F10 cells were euthanized with Zoletil-Rompun mixture. Before cardiac perfusion, fluorescence-conjugated *Lycopersicon esculentum* lectin (BioActs, Korea) was injected to label blood vessels. Mice were perfused with PBS and 4% formaldehyde via the myocardium, and lungs were isolated. The lungs were then incubated in 4% formaldehyde for 24 hours at 4°C. Tissue clearing was performed to acquire 3D structural images using a Binaree Tissue Clearing Kit (Binaree, Korea) according to the manufacturer's instructions. For counts of neutrophils within 50 μm from the boundaries of metastatic foci, metastatic foci with similar size to be analyzed were randomly selected in 3D. Then, three cross sections for each selected focus were randomly chosen in 2D, and neutrophils within 50 μm of these metastatic foci were counted. For counts of neutrophils inside the metastatic foci, three metastatic foci with similar size were arbitrarily chosen. Each selected focus was volumized using software, and the colocalized neutrophils were counted.

Imaging data analysis

Intravital imaging data were obtained and analyzed using Volocity (PerkinElmer, MA, USA, Waltham, USA), Imaris (BITPlan, Switzerland), and Fiji (NIH) software. All data are expressed as the mean ± SEM.

Statistical analysis

Data were analyzed with GraphPad Prism software version 5 (GraphPad Software). Two groups were compared using Student's *t* test. Comparisons of more than two groups were analyzed by one-way analysis of variance (ANOVA) followed by Dunnett's multiple comparisons test. Data are expressed as mean ± SEM for in vivo mouse tumor model. Statistical significance was defined as $P < 0.05$.

SUPPLEMENTARY MATERIALS

Supplementary material for this article is available at http://advances.sciencemag.org/cgi/content/full/6/45/eabc4882/DC1

View/request a protocol for this paper from *Bio-protocol*.

REFERENCES AND NOTES

1. D. F. Quail, J. A. Joyce, Microenvironmental regulation of tumor progression and metastasis. *Nat. Med.* **19**, 1423–1437 (2013).
2. H. Peinado, H. Zhang, I. R. Matei, B. Costa-Silva, A. Hoshino, G. Rodrigues, B. Psaila, R. N. Kaplan, J. F. Bromberg, Y. Kang, M. J. Bissell, T. R. Cox, A. J. Giaccia, J. T. Erler, S. Hiratsuka, C. M. Ghajar, D. Lyden, Pre-metastatic niches: Organ-specific homes for metastases. *Nat. Rev. Cancer* **17**, 302–317 (2017).
3. G. Doglioni, S. Parik, S. M. Fendt, Interactions in the (Pre)metastatic niche support metastasis formation. *Front. Oncol.* **9**, 219 (2019).
4. R. N. Kaplan, R. D. Riba, S. Zacharoulis, A. H. Bramley, L. Vincent, C. Costa, D. D. MacDonald, D. K. Jin, K. Shido, S. A. Kerns, Z. Zhu, D. Hicklin, Y. Wu, J. L. Port, N. Altorki, E. R. Port, D. Ruggero, S. V. Shmelkov, K. K. Jensen, S. Rafii, D. Lyden, VEGFR1-positive haematopoietic bone marrow progenitors initiate the pre-metastatic niche. *Nature* **438**, 820–827 (2005).
5. A. C. Obenauf, J. Massague, Surviving at a distance: Organ-specific metastasis. *Trends in cancer* **1**, 76–91 (2015).
6. G. Hajishengallis, T. Chavakis, DEL-1-regulated immune plasticity and inflammatory disorders. *Trends Mol. Med.* **25**, 444–459 (2019).
7. E. Y. Choi, E. Chavakis, M. A. Czabanka, H. F. Langer, L. Fraemohs, M. Economopoulou, R. K. Kundu, A. Orlandi, Y. Y. Zheng, D. A. Prieto, C. M. Ballantyne, S. L. Constant, W. C. Aird, T. Papayannopoulou, C. G. Gahmberg, M. C. Udey, P. Vajkoczy, T. Quertermous, S. Dimmeler, C. Weber, T. Chavakis, Del-1, an endogenous leukocyte-endothelial adhesion inhibitor, limits inflammatory cell recruitment. *Science* **322**, 1101–1104 (2008).
8. S. Nourshargh, P. L. Hordijk, M. Sixt, Breaching multiple barriers: Leukocyte motility through venular walls and the interstitium. *Nat. Rev. Mol. Cell Biol.* **11**, 366–378 (2010).
9. K. Ley, C. Laudanna, M. I. Cybulsky, S. Nourshargh, Getting to the site of inflammation: The leukocyte adhesion cascade updated. *Nat. Rev. Immunol.* **7**, 678–689 (2007).
10. Y. Y. Kang, D. Y. Kim, S. H. Lee, E. Y. Choi, Deficiency of developmental endothelial locus-1 (Del-1) aggravates bleomycin-induced pulmonary fibrosis in mice. *Biochem. Biophys. Res. Commun.* **445**, 369–374 (2014).
11. E. Y. Choi, J. H. Lim, A. Neuwirth, M. Economopoulou, A. Chatzigeorgiou, K. J. Chung, S. Bittner, S. H. Lee, H. Langer, M. Samus, H. Kim, G. S. Cho, T. Ziemssen, K. Bdeir, E. Chavakis, J. Y. Koh, L. Boon, K. Hosur, S. R. Bornstein, S. G. Meuth, G. Hajishengallis, T. Chavakis, Developmental endothelial locus-1 is a homeostatic factor in the central nervous system limiting neuroinflammation and demyelination. *Mol. Psychiatry* **20**, 880–888 (2015).
12. M. A. Eskan, R. Jotwani, T. Abe, J. Chmelar, J. H. Lim, S. Liang, P. A. Ciero, J. L. Krauss, F. Li, M. Rauner, L. C. Hofbauer, E. Y. Choi, K. J. Chung, A. Hashim, M. A. Curtis, T. Chavakis, G. Hajishengallis, The leukocyte integrin antagonist Del-1 inhibits IL-17-mediated inflammatory bone loss. *Nat. Immunol.* **13**, 465–473 (2012).
13. N. K. Altorki, G. J. Markowitz, D. Gao, J. L. Port, A. Saxena, B. Stiles, T. McGraw, V. Mittal, The lung microenvironment: An important regulator of tumour growth and metastasis. *Nat. Rev. Cancer* **19**, 9–31 (2019).
14. J. Budczies, M. von Winterfeld, F. Klauschen, M. Bockmayr, J. K. Lennerz, C. Denkert, T. Wolf, A. Warth, M. Dietel, I. Anagnostopoulos, W. Weichert, D. Wittschieber, A. Stenzinger, The landscape of metastatic progression patterns across major human cancers. *Oncotarget* **6**, 570–583 (2015).
15. D. L. Kinsey, An experimental study of preferential metastasis. *Cancer* **13**, 674–676 (1960).
16. T. El Rayes, R. Catena, S. Lee, M. Stawowczyk, N. Joshi, C. Fischbach, C. A. Powell, A. J. Dannenberg, N. K. Altorki, D. Gao, V. Mittal, Lung inflammation promotes metastasis through neutrophil protease-mediated degradation of Tsp-1. *Proc. Natl. Acad. Sci. U.S.A.* **112**, 16000–16005 (2015).
17. S. H. Lee, D. Y. Kim, F. Jing, H. Kim, C. O. Yun, D. J. Han, E. Y. Choi, Del-1 overexpression potentiates lung cancer cell proliferation and invasion. *Biochem. Biophys. Res. Commun.* **468**, 92–98 (2015).
18. H. Xia, J. Chen, M. Shi, H. Gao, K. Sekar, V. P. Seshachalam, L. L. Ooi, K. M. Hui, EDIL3 is a novel regulator of epithelial-mesenchymal transition controlling early recurrence of hepatocellular carcinoma. *J. Hepatol.* **63**, 863–873 (2015).
19. S. H. Jiang, Y. Wang, J. Y. Yang, J. Li, M. X. Feng, Y. H. Wang, X. M. Yang, P. He, G. A. Tian, X. X. Zhang, Q. Li, X. Y. Cao, Y. M. Huo, M. W. Yang, X. L. Fu, J. Li, D. J. Liu, M. Dai, S. Y. Wen, J. R. Gu, J. Hong, R. Hua, Z. G. Zhang, Y. W. Sun, Overexpressed EDIL3 predicts poor prognosis and promotes anchorage-independent tumor growth in human pancreatic cancer. *Oncotarget* **7**, 4226–4240 (2016).
20. C. Khanna, K. Hunter, Modeling metastasis in vivo. *Carcinogenesis* **26**, 513–523 (2005).
21. T. Kitamura, B. Z. Qian, J. W. Pollard, Immune cell promotion of metastasis. *Nat. Rev. Immunol.* **15**, 73–86 (2015).
22. A. Lopez-Soto, S. Gonzalez, M. J. Smyth, L. Galluzzi, Control of metastasis by NK cells. *Cancer Cell* **32**, 135–154 (2017).
23. L. B. Merzoug, S. Marie, N. Satoh-Takayama, S. Lesjean, M. Albanesi, H. Luche, H. J. Fehling, J. P. Di Santo, C. A. Vosshenrich, Conditional ablation of NKp46+ cells using a novel Ncr1(greenCre) mouse strain: NK cells are essential for protection against pulmonary B16 metastases. *Eur. J. Immunol.* **44**, 3380–3391 (2014).
24. M. W. L. Teng, D. M. Andrews, N. McLaughlin, B. von Scheidt, S. F. Ngiow, A. Moller, G. R. Hill, Y. Iwakura, M. Oft, M. J. Smyth, IL-23 suppresses innate immune response independently of IL-17A during carcinogenesis and metastasis. *Proc. Natl. Acad. Sci. U.S.A.* **107**, 8328–8333 (2010).
25. Z. Dong, M. E. Cruz-Munoz, M. C. Zhong, R. Chen, S. Latour, A. Veillette, Essential function for SAP family adaptors in the surveillance of hematopoietic cells by natural killer cells. *Nat. Immunol.* **10**, 973–980 (2009).
26. T. Yamamoto, K. Kawada, Y. Itatani, S. Inamoto, R. Okamura, M. Iwamoto, E. Miyamoto, T. F. Chen-Yoshikawa, H. Hirai, S. Hasegawa, H. Date, M. M. Taketo, Y. Sakai, Loss of SMAD4 promotes lung metastasis of colorectal cancer by accumulation of CCR1+ tumor-associated neutrophils through CCL15-CCR1 axis. *Clin. Cancer Res.* **23**, 833–844 (2017).
27. S. B. Coffelt, M. D. Wellenstein, K. E. de Visser, Neutrophils in cancer: Neutral no more. *Nat. Rev. Cancer* **16**, 431–446 (2016).
28. S. K. Wculek, I. Malanchi, Neutrophils support lung colonization of metastasis-initiating breast cancer cells. *Nature* **528**, 413–417 (2015).
29. S. B. Coffelt, K. Kersten, C. W. Doornebal, J. Weiden, K. Vrijland, C. S. Hau, N. J. M. Verstegen, M. Ciampricotti, L. Hawinkels, J. Jonkers, K. E. de Visser, IL-17-producing γδ T cells and neutrophils conspire to promote breast cancer metastasis. *Nature* **522**, 345–348 (2015).

30. L. Chiossone, J. Chaix, N. Fuseri, C. Roth, E. Vivier, T. Walzer, Maturation of mouse NK cells is a 4-stage developmental program. *Blood* **113**, 5488–5496 (2009).
31. A. Spiegel, M. W. Brooks, S. Houshyar, F. Reinhardt, M. Ardolino, E. Fessler, M. B. Chen, J. A. Krall, J. DeCock, I. K. Zervantonakis, A. Iannello, Y. Iwamoto, V. Cortez-Retamozo, R. D. Kamm, M. J. Pittet, D. H. Raulet, R. A. Weinberg, Neutrophils suppress intraluminal NK cell-mediated tumor cell clearance and enhance extravasation of disseminated carcinoma cells. *Cancer Discov.* **6**, 630–649 (2016).
32. M. J. McGeachy, D. J. Cua, Th17 cell differentiation: The long and winding road. *Immunity* **28**, 445–453 (2008).
33. C. Jin, G. K. Lagoudas, C. Zhao, S. Bullman, A. Bhutkar, B. Hu, S. Ameh, D. Sandel, X. S. Liang, S. Mazzilli, M. T. Whary, M. Meyerson, R. Germain, P. C. Blainey, J. G. Fox, T. Jacks, Commensal microbiota promote lung cancer development via γδ T cells. *Cell* **176**, 998–1013.e16 (2019).
34. T. Maekawa, K. Hosur, T. Abe, A. Kantarci, A. Ziogas, B. Wang, T. E. Van Dyke, T. Chavakis, G. Hajishengallis, Antagonistic effects of IL-17 and D-resolvins on endothelial Del-1 expression through a GSK-3β-C/EBPβ pathway. *Nat. Commun.* **6**, 8272 (2015).
35. B. Psaila, D. Lyden, The metastatic niche: Adapting the foreign soil. *Nat. Rev. Cancer* **9**, 285–293 (2009).
36. K. Uchida, D. C. Beck, T. Yamamoto, P. Y. Berclaz, S. Abe, M. K. Staudt, B. C. Carey, M. D. Filippi, S. E. Wert, L. A. Denson, J. T. Puchalski, D. M. Hauck, B. C. Trapnell, GM-CSF autoantibodies and neutrophil dysfunction in pulmonary alveolar proteinosis. *N. Engl. J. Med.* **356**, 567–579 (2007).
37. F. Liu, J. Poursine-Laurent, H. Y. Wu, D. C. Link, Interleukin-6 and the granulocyte colony-stimulating factor receptor are major independent regulators of granulopoiesis in vivo but are not required for lineage commitment or terminal differentiation. *Blood* **90**, 2583–2590 (1997).
38. D. F. Quail, O. C. Olson, P. Bhardwaj, L. A. Walsh, L. Akkari, M. L. Quick, I. C. Chen, N. Wendel, N. Ben-Chetrit, J. Walker, P. R. Holt, A. J. Dannenberg, J. A. Joyce, Obesity alters the lung myeloid cell landscape to enhance breast cancer metastasis through IL5 and GM-CSF. *Nat. Cell Biol.* **19**, 974–987 (2017).
39. F. Veglia, V. A. Tyurin, M. Blasi, A. De Leo, A. V. Kossenkov, L. Donthireddy, T. K. J. To, Z. Schug, S. Basu, F. Wang, E. Ricciotti, C. DiRusso, M. E. Murphy, R. H. Vonderheide, P. M. Lieberman, C. Mulligan, B. Nam, N. Hockstein, G. Masters, M. Guarino, C. Lin, Y. Nefedova, P. Black, V. E. Kagan, D. I. Gabrilovich, Fatty acid transport protein 2 reprograms neutrophils in cancer. *Nature* **569**, 73–78 (2019).
40. N. Faust, F. Varas, L. M. Kelly, S. Heck, T. Graf, Insertion of enhanced green fluorescent protein into the lysozyme gene creates mice with green fluorescent granulocytes and macrophages. *Blood* **96**, 719–726 (2000).
41. T. Chtanova, M. Schaeffer, S. J. Han, G. G. van Dooren, M. Nollmann, P. Herzmark, S. W. Chan, H. Satija, K. Camfield, H. Aaron, B. Striepen, E. A. Robey, Dynamics of neutrophil migration in lymph nodes during infection. *Immunity* **29**, 487–496 (2008).
42. A. Rydstrom, M. J. Wick, Monocyte recruitment, activation, and function in the gut-associated lymphoid tissue during oral Salmonella infection. *J. Immunol.* **178**, 5789–5801 (2007).
43. Z. Granot, E. Henke, E. A. Comen, T. A. King, L. Norton, R. Benezra, Tumor entrained neutrophils inhibit seeding in the premetastatic lung. *Cancer Cell* **20**, 300–314 (2011).
44. Z. G. Fridlender, J. Sun, S. Kim, V. Kapoor, G. Cheng, L. Ling, G. S. Worthen, S. M. Albelda, Polarization of tumor-associated neutrophil phenotype by TGF-beta: "N1" versus "N2" TAN. *Cancer Cell* **16**, 183–194 (2009).
45. T. O. Jensen, H. Schmidt, H. J. Møller, F. Donskov, M. Høyer, P. Sjoegren, I. J. Christensen, T. Steiniche, Intratumoral neutrophils and plasmacytoid dendritic cells indicate poor prognosis and are associated with pSTAT3 expression in AJCC stage I/II melanoma. *Cancer* **118**, 2476–2485 (2012).
46. J. Cursons, F. Souza-Fonseca-Guimaraes, M. Foroutan, A. Anderson, F. Hollande, S. Hediyeh-Zadeh, A. Behren, N. D. Huntington, M. J. Davis, A gene signature predicting natural killer cell infiltration and improved survival in melanoma patients. *Cancer Immunol. Res.* **7**, 1162–1174 (2019).
47. H. J. Kwon, G. E. Choi, S. Ryu, S. J. Kwon, S. C. Kim, C. Booth, K. E. Nichols, H. S. Kim, Stepwise phosphorylation of p65 promotes NF-κB activation and NK cell responses during target cell recognition. *Nat. Commun.* **7**, 11686 (2016).
48. G. E. Choi, S. Y. Yoon, J. Y. Kim, D. Y. Kang, Y. J. Jang, H. S. Kim, Autophagy deficiency in myeloid cells exacerbates eosinophilic inflammation in chronic rhinosinusitis. *J. Allergy Clin. Immunol.* **141**, 938–950.e12 (2018).
49. D. Kreisel, R. G. Nava, W. Li, B. H. Zinselmeyer, B. Wang, J. Lai, R. Pless, A. E. Gelman, A. S. Krupnick, M. J. Miller, In vivo two-photon imaging reveals monocyte-dependent neutrophil extravasation during pulmonary inflammation. *Proc. Natl. Acad. Sci. U.S.A.* **107**, 18073–18078 (2010).
50. M. R. Looney, E. E. Thornton, D. Sen, W. J. Lamm, R. W. Glenny, M. F. Krummel, Stabilized imaging of immune surveillance in the mouse lung. *Nat. Methods* **8**, 91–96 (2011).

Acknowledgments: We thank Y. K. Kim and G. E. Choi for support and helpful discussion and H. J. Kim and J.-Y. Kim for technical assistance. **Funding:** This work was supported by grants from the National Research Foundation funded by the Ministry of Science and ICT (MSIT) of the government of Korea (2019R1A2C2006475 to H.S.K., 2020R1F1A1068935 to E.Y.C., and 2019R1A2C2008481 to Y.-M.H.); by the Intelligent Synthetic Biology Center of the Global Frontier Project (2013-0073185 to H.S.K.); by an MRC grant (2018R1A5A2020732 to H.S.K.) funded by the Korean government (MSIT); partly by grants (nos. 2017-516 and 2019-516 to E.Y.C.) from the Asan Institute for Life Sciences, Asan Medical Center, Seoul, Korea; and by a grant from the NIH (NIH R01 HL107386 to M.R.L.). **Author contributions:** Y.-M.H., S.-U.S., W.S.C., H.-J.K., D.-Y.K., S.J., G.-Y.K., E.Y., M.K., and H.J.R. were involved in data acquisition. Y.-M.H., M.R.L., E.Y.C., and H.S.K. were involved in data analysis and interpretation. M.R.L. helped design studies with intravital imaging. Y.-M.H., S.-U.S., E.Y.C., and H.S.K. contributed to the conceptual design of the study and writing of the manuscript with input from all coauthors. **Competing interests:** The authors declare that they have no competing interests. **Data and materials availability:** All data needed to evaluate the conclusions in the paper are present in the paper and/or the Supplementary Materials. Additional data related to this paper may be requested from the authors.

Submitted 27 April 2020
Accepted 18 September 2020
Published 6 November 2020
10.1126/sciadv.abc4882

Citation: Y.-M. Hyun, S.-U. Seo, W. S. Choi, H.-J. Kwon, D.-Y. Kim, S. Jeong, G.-Y. Kang, E. Yi, M. Kim, H. J. Ryu, M. R. Looney, E. Y. Choi, H. S. Kim, Endogenous DEL-1 restrains melanoma lung metastasis by limiting myeloid cell–associated lung inflammation. *Sci. Adv.* **6**, eabc4882 (2020).